Simulation of Airlift Pumps for Moderate-Depth Water Wells

A. NENES[1], D. ASSIMACOPOULOS[*1], N. MARKATOS[1] and G. KARYDAKIS[2]

[1] National Technical University of Athens, Department of Chemical Engineering, Sector II, Iroon Polytechniou 9, GR 157-73, Zografou, Athens, Greece

[2] IGME, Department of Geothermy, Zagoras 16, GR 115-27, Athens, Greece

Abstract

A model is developed which simulates water airlift pumps. The water flow rate can be predicted for a given airlift system, or, the required air flow can be estimated for a desired water flow rate. Predictions of the model were compared with a series of experiments performed by the Institute of Geological Research and were found to be in good agreement. The predictions were far superior to those of model found in the literature.

Published in Technika Chronika, **14**, 1-20 (1996). *Translated from the original Greek text.*

**Corresponding author.Email contacts: nenes@its.caltech.edu, assim@chemeng.ntua.gr*

1. Introduction

Airlift pumping is used in specialized applications, where more conventional and efficient pumps fail to operate. Despite the low energy efficiency of airlift pumping, their simplicity and lack of moving mechanical parts are two important advantages which make them useful for applications such as pumping corrosive fluids and in geothermal wells, [1]. It is also used for pumping of hydrocarbons, viscuous fluids [2], in bioreactors [3,4], and for seabed mining [5].

Simulation of these pumping systems can be achieved by using empirical correlations [6], or by using mathematical models based on a first-principle approach [7,8,9]. This paper aims in developing a new model, referred to as the *integral model*, which uses a combination of a first principal approach and experimental correlations. This model can address two basic airlift design problems:

- Calculation of the water pumping rate for a given air flow rate, and,
- Calculation of the air flow rate needed to obtain a prescribed liquid pumping rate.

It is relatively easy to extend the integral model in order to address more complicated design problems, such as optimization of the air compressor and pipe diameters, and simulation of tapered pipe (variable diameter) systems.

To verify the new model, simulations are compared with experimental measurements and with the predictions of another model currently in use, the *mean void fraction model*, [7,8]. In subsequent sections, the mean void fraction model and integral models are presented. The two models are then used to reproduce a series of measurements taken by the Greek Institute of Mineorological Research (IGME) for a series of water wells.

2. Nomenclature

a	Volume fraction (void fraction is air volume fraction)
A_1	Suction pipe cross section (water flow)
A_2	Upriser pipe cross section (two phase flow mixture)
D	Diameter of outer pipe
D_1	Equivalent diameter of suction pipe
D_2	Equivalent diameter of upriser
J''	Momentum flux, $M_i^2/(a_i \rho_i A^2),\ i = g,l$
L	Length of inner pipe, $l_s + l_d + l_e$
M	Mass flow rate
N	Number of cells
P	Pressure
R	Universal gas constant
R^*	Specific gas constant: R/(molecular weight)
Re	Reynolds number
T	Temperature
U_{gs},U_{ls}	Superficial gas and liquid velocity, $V_i/A_2,\ i = g,l$
V	Volume flow rate
a	Volume fraction
d	Diameter of inner pipe
f_m	Friction coefficient
g	Gravity acceleration
l_d	Length of upriser above the water level
l_e	Length of suction pipe

l_s	Length of upriser below the water level
M	Mass flux, $M_i/(a_i A)$, $i = g,l$
Δz	$(l_s + l_d)/N$
ε	Convergence criterion for iterative procedures
μ	Viscosity
ξ	Entrance factor
ρ	Density

Subscripts-superscripts

1, 2, i	Property at point 1, 2 or i
f	Friction
g,l	Gas or liquid phase property
k	Property at cell face *k*
m	Average property of cell

3. Description of Airlift Pumping - Mean Void Fraction Model

3.1. Description of airlift pumping

Figure 3.1 displays a typical airlift pumping system. It is composed of a water suction pipe, length l_e, and an upriser section, part of which, l_s, is submerged, and the remainder, l_d, is above the water level. Compressed air is delivered at point *i* (injection point) either externally, or through an internal pipe (Figure 3.2). The first configuration is known as external delivery (or external airline) system, while the second is internal delivery (or internal airline) system. In the

suction pipe, between points *1* and *i*, there is only water flowing, while between points *i* and *2* (upriser) there is a two phase water-air flow.

External delivery systems are more energy efficient than internal delivery systems, but occupy more space within the well (because of the air delivery pipe). This limits the diameter of the upriser that can be used. Internal delivery systems, despite the larger friction losses (which decreases the energy efficiency) are more versatile, and easier to install and operate. If the well water level fluctuates with time, the internal pipe length can easily be adjusted to ensure optimal operating conditions. This is much harder to achieve with external delivery systems.

Generally, the water well level is not constant, but tends to drop with increasing pumping rate. Furthermore, the water level drops slightly with time at a constant pumping rate. With this in mind, we define a *non-operational* (or idle) water level (when the pump is not in use) and an *operational water level* (when the pump is in use). Subsequently, the water level during operation will be referred simply as water level.

The cross section of the suction pipe is denoted as A_1, while the cross section of the two phase flow (upriser) cross section is A_2. In external delivery systems, all of the upriser cross section is occupied by the two-phase mixture (Figure 3.2). Slug flow is the desired flow regime in the upriser, because frictional losses become minimum, while water pumping rates are still large, [7].

3.2. Mean void fraction model

Kato et al [8], developed a simple model for airlift pumps. This model is derived by applying a momentum balance throughout the upriser, assuming that the void fraction, a_g, remains constant:

$$a_g = \frac{\overline{V}_g}{\overline{V}_g + V_l + 0.35\, A_2 \sqrt{g\, D_2}} \tag{3.1}$$

where $\overline{V}_g$ is the average air volumetric flow rate, calculated assuming isothermal expansion of air between points *2* and *i*:

$$\overline{V}_g = V_{g,2} \left(\frac{P_2}{P_i - P_2} \right) \ln \frac{P_i}{P_2} \tag{3.2}$$

The pressure at *i*, P_i is calculated by using the algorithm of paragraph 4.2. The water mass pumping rate M_l (or air delivery rate M_g) can be calculated by solving the following algebraic equation:

$$\frac{2V_l^2}{g} \frac{f_{mix}}{L} \left[\frac{l_e}{D_1 A_1^2} + \frac{l_s + l_d}{D_2 A_2^2} (1 - a_g)^{-1.75} + \frac{1}{2} \left(\frac{1}{1 - a_g} - \frac{3}{4} \right) \right] + \frac{l_d}{l_d + l_s} - a_g = 0 \tag{3.3}$$

where

$$f_{mix} = 0.079\ Re_{mix}^{-0.25} \quad \text{and} \quad Re_{mix} = \frac{M_l + M_g}{A_2\ \mu_l}\ D_2 \tag{3.4}$$

The mean void fraction model is limited mainly because:

- Only one flow regime (slug flow) is assumed to exist throughout the upriser. As a consequence, flow transitions are not considered, which limits the applicability of the model to wells up to 11 m deep.

- The correlations proposed for calculating volume fraction and friction losses are of limited accuracy.

4. Integral Model

The integral model improves upon the mean void fraction model by addressing the two limitations previously noted. First, flow regimes within the upriser are allowed to vary, and are predicted by using an appropriate flow regime map. Second, the properties of the two-phase mixture within the upriser are allowed to vary, by dividing the upriser into subsections (or "cells"). In each of these cells, mean properties (such as pressure and void fraction) are considered representative of the cell, and differ from properties of adjacent cells. A momentum balance is applied to each cell, using correlations for friction losses and void fraction. Eventually, a system of algebraic equations is obtained, and is solved using the two known pressure boundary conditions at points *1* and *2*.

4.1. Flow in the upriser

As previously stated, the flow field within the upriser is divided into sections ("cells"). Every cell defines two interfaces, one at the "bottom" (entrance) of the cell, and one at the "top" (exit). Numbering of the cells and interfaces start from point *i* and increase toward point *2* (Figure 4.1). The two-phase mixture enters cell k from the k interface and exits through the $k+1$ interface. The physical properties (such as void fraction and pressure) of both phases are defined at each interface, while properties inside each cell are the mean of k and $k+1$ interface values. For interface $k=1$, pressure is equal to P_i, while at $k=N+1$, pressure is equal to P_2. A momentum balance is applied to each cell, which for steady state is expressed as:

$$(exit\ \ flux) - (entrance\ \ flux) = (applied\ \ forces) \tag{4.1}$$

The forces applied are the pressure drop, gravitational forces and friction. These are calculated as:

Pressure drop, ΔP_k

$$- \Delta P_k = - \left(P_{k+1} - P_k \right) \tag{4.2}$$

Gravitational (hydrostatic) forces, B_k

$$B_k = g \int_{z_k}^{z_{k+1}} \left(a_g \, \rho_g \; + \; a_l \, \rho_l \right) dz \approx g \left[a_{g,m} \, \rho_{g,m} \; + \; a_{l,m} \, \rho_l \right] \Delta z \tag{4.3a}$$

$$a_{g,m} = 0.5 \left(a_{g,k} + a_{g,k+1} \right), \;\; a_{l,m} = 1.0 - a_{g,m} \, , \; \rho_{g,m} = 0.5 \left(\rho_{g,k} + \rho_{g,k+1} \right) \tag{4.3b}$$

The void fraction at the interfaces is calculated from correlations which are presented in section 4.3.

Friction, T_k

Friction forces are calculated from correlations and are expressed in terms of a pressure drop:

$$T_k \; = \int_{z_k}^{z_{k+1}} \left(\frac{dP}{dz} \right)_f dz \approx \left(\frac{dP}{dz} \right)_f \; \Delta z \tag{4.4}$$

Rate of change of momentum flux

Momentum enters through the k interface and exits from interface $k+1$. So, the rate of change of momentum flux $\Delta J_k''$ is

$$\Delta J_k'' = J_{k+1}'' - J_k'' \tag{4.5a}$$

$$J_{k+1}'' = J_{g,k+1}'' + J_{l,k+1}'' = \frac{M_{g,k+1}^2}{a_{g,k+1}\,\rho_{g,k+1}\,A_2^2} + \frac{M_{l,k+1}^2}{a_{l,k+1}\,\rho_l\,A_2^2}$$

$$J_k'' = J_{g,k}'' + J_{l,k}'' = \frac{M_{g,k}^2}{a_{g,k}\,\rho_{g,k}\,A_2^2} + \frac{M_{l,k}^2}{a_{l,k}\,\rho_l\,A_2^2} \tag{4.5b}$$

If the air is assumed ideal, the air volumetric flow rate $V_{g,k}$, and density $\rho_{g,k}$, are given by

$$V_{g,k} = \frac{T_k}{P_k}\left(\frac{P_o\ V_{go}}{T_o}\right) \tag{4.6}$$

$$\rho_{g,k} = \frac{P_k}{R^*\ T_k} \tag{4.7}$$

R^* for air is 0.2867 J.kg^{-1}.K^{-1}, while V_{g0} is the air compressor delivery rate at the reference conditions T_o, P_o (free air delivery).

The mean cell properties are used for calculating the void fraction and friction (from the appropriate correlations). These correlations are generally functions of volumetric flow rate and density (section 4.3):

$$\left(\frac{dP}{dz}\right)_f = f_1\{\dot{V}_{g,m},\ \rho_{g,m}\} \tag{4.8}$$

$$a_{g,m} = f_2\{\dot{V}_{g,m},\ \rho_{g,m}\} \tag{4.9}$$

Substituting (4.2) to (4.5b) in (4.1), and solving for P_k yields

$$P_k = P_{k+1} + \left(\frac{M_{g,k+1}^2}{a_{g,k+1}\,\rho_{g,k+1}\,A_2^2} + \frac{M_{l,k+1}^2}{a_{l,k+1}\,\rho_l\,A_2^2} - \frac{M_{g,k}^2}{a_{g,k}\,\rho_{g,k}\,A_2^2} - \frac{M_{l,k}^2}{a_{l,k}\,\rho_l\,A_2^2} \right)$$

$$+ g(\,a_{g,m}\,\rho_{g,m} + a_{l,m}\,\rho_l\,)\,\Delta z + \left(\frac{dP}{dz}\right)_f \Delta z \tag{4.10}$$

4.2. Flow in the suction pipe

A simple momentum balance (Bernoulli equation) is applied between points *1* and *i*:

$$P_i = P_1 - \rho_l\, g\, l_e + \left(\frac{dP}{dz}\right)_{f,l} l_e \tag{4.11}$$

Pressure at *1* is equal to the hydrostatic pressure (as dictated by the water level in the well) less the friction losses at the entrance of the suction pipe:

$$P_1 = P_2 + \rho_l\, g\,(\,l_s + l_e\,) + (Friction) \tag{4.12}$$

The entrance friction losses are calculated as:

$$(Friction) = -\,\xi\,\frac{M_l^2}{2\,\rho_l\,A_1^2} \tag{4.13}$$

where ξ, known as entrance factor, is approximately 0.5 for the geometry considered.

Substituting the expression for P_1 from Equations (4.12), (4.13) to (4.11), and solving for P_i yields:

$$P_i = P_2 + \rho_l\, g\, l_s - \xi\,\frac{M_l^2}{2\,\rho_l\,A_1^2} + \left(\frac{dP}{dz}\right)_{f,l} l_e \tag{4.14}$$

friction losses inside the suction pipe are computed from

$$\left(\frac{dP}{dz}\right)_{f,l} = -f_m \frac{4}{D_1}\frac{M_l^2}{2\rho_l A_1^2} \tag{4.15}$$

where

$$f_m = \begin{cases} 16/\mathrm{Re}_l & \mathrm{Re} \le 2000 \\ 0.079\,\mathrm{Re}_l^{-0.25} & \mathrm{Re} > 2000 \end{cases} \tag{4.16}$$

where Re_l is the Reynolds of the water phase in the suction pipe.

4.3. Flow regimes, friction and void fraction correlations

The correlations used for calculating the void fraction and friction losses in equations (4.8), (4.9) depend on the flow regime existing in each cell. To determine the flow regime, a flow regime map, [10] is used (Figure 4.2). When flow regimes change, the correlations used change; this may introduce discontinuities in the friction and void fraction. As a result, convergence problems might be encountered in the solution process. To address this, a transition region (and not a transition line) is assumed between two flow regimes. Inside this region, properties are a weighted average of the values calculated for both regimes.

Void fraction correlations used

Lockhart-Martinelli, [11]

$$a_g = \left(1 + X^{0.8}\right)^{-0.378}$$

the Lockhart-Martinelli parameter, X , is given by [12]

$$X^2 = \left(\frac{M_l}{M_g}\right)^{1.8}\left(\frac{\rho_g}{\rho_l}\right)\left(\frac{\mu_l}{\mu_g}\right)^{0.2} \tag{4.17}$$

Friction correlations used

Bubble flow, [13]

$$\left(\frac{dP}{dz}\right)_f = -2\frac{f_T\,(U_{gs}+U_{ls})^2\,\rho_l}{D_2}$$

$$f_T = 0.046\ N_{Re}^{-0.20}\ ,\quad N_{Re} = \frac{D_2(U_{gs}+U_{ls})\,\rho_l}{\mu_l}$$

Slug flow, (Freidel), [14]

$$\left(\frac{dP}{dz}\right)_f = \Phi_{LO}^2\left(\frac{dP}{dz}\right)_{LO}$$

where $$\Phi_{LO}^2 = E + \frac{3.24\ F\ H}{Fr^{0.045}\,We^{0.035}}$$

$$Fr = \frac{m^2}{g\ D_2\ \rho_{TP}} \qquad We = \frac{m^2\,D_2}{\rho_{TP}\,\sigma} \qquad \rho_{TP} = \left(\frac{\chi}{\rho_g} + \frac{1-\chi}{\rho_l}\right)^{-1}$$

$$H = \left(\frac{\rho_l}{\rho_g}\right)^{0.91}\left(\frac{\mu_g}{\mu_l}\right)^{0.19}\left(1-\frac{\mu_g}{\mu_l}\right)^{0.71} \qquad F = \chi^{0.78}\ (1-\chi)^{0.224}$$

$$E = (1-\chi)^2 + \chi^2\left[\frac{\rho_l}{\rho_g}\left(\frac{\mu_g}{\mu_l}\right)^{1/4}\right] \qquad \chi = \frac{M_g}{M_g + M_l}$$

Churn and annular flow (Kern), [12]

$$\left(\frac{dP}{dz}\right)_f = \Phi_{LO}^2\left(\frac{dP}{dz}\right)_{LO}\ ,\quad \Phi_{LO} = aX^b$$

where X is the Martinelli parameter, (Equation 4.17) and for *churn flow*

$$a = \frac{14.2}{\left(\frac{M_l}{1.6404\,\pi\,D_2}\right)^{0.1}}, \quad b = 0.75$$

for *annular flow*

$$a = 4.8 - 0.3125\left(\frac{D_2}{0.0254}\right), \quad b = 0.343 - 0.021\left(\frac{D_2}{0.0254}\right)$$

where

$$\left(\frac{dP}{dz}\right)_{LO} = -\frac{2\,f_{LO}\,m^2}{D_2\,\rho_l} \qquad f_{LO} = 0.079\,N_{Re_{LO}}^{-0.25} \qquad N_{Re_{LO}} = \frac{m\,D_2}{\mu_l} \qquad m = \frac{M_g + M_l}{A_2}$$

4.4. Solution algorithm

The momentum equation (4.10) for each cell and equation (4.14) consists a non-linear system of $N+1$ equations with $N+1$ unknowns (N-1 P_k's, Pi and one of M_l or M_g). The solution algorithm is the following:

1. An estimate for M_l (or M_g) is made.

2. The system of the equations (4.10) is solved: (i) For every k, equation (4.10) is solved by the bisection method, [30]. (ii) Solution of (4.10) for cell $k=1$, yields the pressure P_i for the estimated M_l (or M_g).

3. P_i is computed from (4.14) for the estimate of M_l (or M_g) made in step 1.

4. If P_i from step 3 is equal to P_i from step 2, then the value of M_l (or M_g) is correct. Otherwise, another estimation is made for M_l (or M_g) and steps 2 through 4 are repeated until $\left|Pi\ (from\ step\ 2) - Pi\ (from\ step\ 3)\right| < \varepsilon \left|Pi\ (from\ step\ 3)\right|$.

In step 2, the system of momentum equations are solved from cell *N*, downward. For the kth cell, the pressure at *k+1* interface is known by the previously solved *k+1* momentum balance. For cell *N*, pressure at the *N+1* interface is known, and equal to the exit pressure (usually assumed 1 atm).

5. Experimental Measurements

The following experimental data was obtained by the Greek Institute of Minerological Research, in a series of experiments taken during 19 Sept. 1988 and 23 Sept. 1988. The data sets were obtained from 3 different wells in the region of Sidirokastron in the Xanthi state. An internal delivery system was used. Overall, 7 sets of measurements were made. In each of these sets, the length of the air delivery pipe was allowed to vary. In all of these measurements, the air compressor used delivered 160 cfm (0.07852 m^3s^{-1}), at pressue P_o=1 atm temperature T_o=40°C. The water level is defined as the length of the submerged external pipe. The data sets are presented in Tables 5.1 to 5.7.

6. Results - Conclusions

A grid of 25 cells along the upriser was used in the simulations. As seen in Figure 6.1, using more cell does not change the solution obtained. It should be noted that the usage of the friction loss and void fraction correlations allows the method to sufficiently resolve the momentum flux along the upriser using only 25 cells, despite that the structure of the two phase flow develops on much smaller spatial scales.

The experimental data and predictions of both integral and void fraction models are presented in Figures 6.2 to 6.8. Table 6.1 presents the mean error of predictions from experiment for each model, where

$$\%\ mean\ error\ = \frac{\sum \left| \frac{M_{l,\mathrm{predict}} - M_{l,\mathrm{exper}}}{M_{l,\mathrm{exper}}} \right|}{number\ of\ measurements} \times 100\,\% \qquad (6.1)$$

The standard deviation is given in the parenthesis. A graphical representation of the deviation between predicted and measured pumping rates is given in Figures 6.9, 6.10 and 6.11.

The integral model reproduces the measurements well, and is always much better results compared to the mean void fraction model. The maximum mean error of the integral model is 29%, while the mean void fraction model gave an error as high as 136%. Besides significantly decreasing the mean error from the measurements, there is also a decrease in the error variability, meaning that the pumping curves are reproduced much closely. The predictions are closest to the experiments, when slug flow is predicted to exist throughout the upriser (sets 1,2 and 4). This is expected, because the Martinelli correlation provides satisfactory predictions in this region [13,15,16]. Relatively large deviations in the slope of the experimental and predicted curves are seen in the seventh measurement set. This can be attributed to the prediction of annular flow in these measurements; for this flow regime type, the Martinelli correlation is not as accurate.

The accuracy of the void fraction correlation is what mainly determines the accuracy of the model. This is because the hydrostatic component (which is linear with respect to void fraction) is the leading order term in the momentum balance of Equation 4.10. Developing more accurate correlations for the void fraction, that can be applied over a larger range of flow regimes, will allow for further improvement of the integral model predictions.

References

1. Ryley D.J., Parker G.J. "Flowing geothermal wells: Cerro Priet wells M.91 and Krafla well KJ-9.1: Computer analysis compared with experimental data", *Int. Conf. on Geothermal Energy*, Florence Italy, May, 1982, pp. 187-196.

2. Deplution Div., Ralph B. Carter Co. "Belched Bubbles hasten Waste Digestion", *Chem. Eng.*, December 18 1967, pp. 58-60

3. Chisti V.,"Assure Bioreactor Sterility", *Chem. Eng. Prog.*, September 1992, pp. 80-85

4. Trystam G., Pigache S. "Modelling and Simulation of a large scale air lift fermenter", *European Symposium on Computer Aided Process Engineering-2*, 1992, pp. 5171-5176

5. Mero J.L.,"Seafloor Minerals: A Chemical Engineeering Challenge", *Chem. Eng. Prog.*, July 1 1968, pp. 73-80

6. Zenz F.A.,"Explore the potential of Air-Lift Pumps and Multiphase", *Chem. Eng. Prog.*, August 1993, pp. 51-56

7. Giot M., "Three phase flow", Chapter 7.2 in Handbook of Multiphase Systems, Hetsroni G. (Editor), Hemisphere-McGraw Hill, Washington, 1982, pp. 7.37-7.43.

8. Kato H., Miyazawa T., Timaya S., Iwasaki T. "A study of an airlift pump for solid particles", *Bull. JSME*, **18**, 1975, pp. 286-294.

9. Casey T.J., *"Water and Wastewater Engineering"*, Oxford University Press, 1992, pp. 181-185

10. Taitel Y., Bornea D., Buckler A.E. "Modelling flow pattern transitions for steady upward gas-liquid flow in vertical tubes", *AIChE Journal*, **26**, 1980, pp. 345-354.

11. Lockhart R.W., Martinelli R.C. "Proposed correlation of data for isothermal two-phase, two-component flow of data in pipes", *Chem. Eng. Progr.*, **45**, 1949, pp. 39-48.

12. Kern R., *Chemical Engineering*, McGraw-Hill, New York, 1975, pp. 145-151.

13. Govier G.W., Aziz A., *The flow of complex mixtures in pipes*, Van Nostrand Reinhold Co., 1972.

14. Friedel L. "Improved friction pressure drop correlations for horizontal and vertical two-phase pipe flow", *European Two Phase Flow Group Meet.*, Ispra, Italy, paper E2, 1979.

15. Wallis G.B., *One dimensional Two-Phase Flow*, McGraw-Hill, New York, 1969.

16. Duckler A.E., Wicks M., Cleveland R.G. "Frictional pressure drop in two-phase flow: A. A comparison of existing correlations for pressure loss and holdup", *AIChE Journal*, Jan. 1964, pp. 38-43.

17. Brennand A.W., Watson A. "Use of the ESDU compilation of two-phase flow correlations for the prediction of well discharge characteristics", *Proc. 9th NZ Geothermal Workshop*, 1987, pp. 65-68.

18. Chisholm D. "Pressure gradients due to friction during the flow of evaporating two-phase mixtures in smooth tubes and channels", *Int. J. Heat and Mass Transfer*, **16**, 1973, pp. 347-348.

19. Delhaye J.M. "Two-phase pipe flow", *Int. Chem. Eng.*, **23**, Jul. 1983, pp. 385-410.

20. Duckler A.E., Wicks M., Cleveland R.G. "Frictional pressure drop in two-phase flow: B. An approach through similiarity analysis", *AIChE Journal*, Jan. 1964, pp. 44-51.

21. Fernandes R.C., Semiat R., Duckler A.E. "Hydrodynamic model for gas-liquid slug flow in vertical tubes", *AIChE Journal*, **29**, Nov. 1983, pp. 981-989.

22. Freeston D.H., Hadgu H. "Modelling of geothermal wells with multiple feed points: a preliminary study", *Proc. 9th NZ Geothermal Workshop*, 1987, pp. 59-64.

23. Gibson A.H., *Hydraylics and its Applications*, 5thed., Constable, London, 1961.

24. Govier G.W., Radford B.A., Dunn J.S.C. "The upwards vertical flow of air-water mixtures", *Can. J. Ch. Eng.*, Aug. 1957, pp. 58-70.

25. Hewitt G.F., Delhaye J.M., Zuber N., *Multiphase Science and Technology*, Hemisphere, New York, 1982.

26. Hjalmars S., "The origin of instability in airlift pumps", *Trans. ASME, J. Appl. Mech.*, **40**, 1973, pp.399-404

27. Ishii M., Zuber N. "Drag coefficient and relative velocity in bubbly, droplet or particulate flows", *AIChE Journal*, **25**, Sept. 1979, pp. 843-855.

28. Leaver J.D., Freeston D.H. "Simplified prediction of output curves for steam wells", *Proc. 9th NZ Geothermal Workshop*, 1987, pp. 55-57.

29. Stenning A.H., Martin C.B. "An analytical and experimental study of airlift pump preformance", *J.Eng.Power*, **90**, 1968, pp. 106-110

30. Press W., Flannery B.P., Teukolsky S.A., Vetterling W.T., *Numerical Recipes*, Cambridge Press, 1982.

31. Todoroki I., Sato Y., Honda T. "Preformance of airlift pumps", *Bull. JSME*, **16**, 1973, pp. 733-741

32. Zuber N., Findlay J.A. "Average volumetric concentration in two phase systems", *J. Heat Transfer*, **87**, 1965, pp. 453-468.

33. J.I.York, J.T.Barberio, M.Samyn, F.A.Zenz, J.A.Zenz "Solve All Column Flows with One Equation", *Chem.Eng.Prog.*, October 1992, pp. 93-98

Table 5.1 First set of measurements, L=46.6m, D=10.16cm, d=2.54cm, water temperature 56°C

Point	Inner pipe length (m)	Water level (m)	Water pumping rate (m^3 h^{-1})
1	45.80	22.70	25.5
2	42.20	22.90	23.0
3	39.20	23.10	19.0
4	36.20	23.20	16.0
5	33.20	23.40	11.0
6	30.20	23.50	6.0

Table 5.2 Second set of measurements, L=46.6m, D=10.16cm, d=1.91cm, water temperature 56°C

Point	Inner pipe length (m)	Water level (m)	Water pumping rate (m^3 h^{-1})
1	46.20	22.80	27.0
2	42.20	22.90	23.0
3	39.20	23.20	20.0
4	36.20	23.40	16.0
5	33.20	23.50	11.0
6	30.20	23.60	5.0

Table 5.3 Third set of measurements, L=46.6m, D=10.16cm, d=1.27cm, water temperature 56°C

Point	Inner pipe length (m)	Water level (m)	Water pumping rate (m^3 h^{-1})
1	36.20	23.40	13.6
2	33.20	23.50	8.2
3	30.20	23.50	4.0

Table 5.4 Fourth set of measurements, L=45.1m, D=10.16cm, d=1.27cm, water temperature 42°C

Point	Inner pipe length (m)	Water level (m)	Water pumping rate (m^3 h^{-1})
1	24.20	40.10	42.0
2	18.20	40.20	34.0
3	12.20	40.50	22.0

Table 5.5 Fifth set of measurements, L=45.1m, D=10.16cm, d=1.91cm, water temperature 42°C

Point	Inner pipe length (m)	Water level (m)	Water pumping rate (m^3 h^{-1})
1	30.20	39.87	48.0
2	24.20	40.18	40.0
3	18.20	40.22	33.0
4	12.20	40.45	22.0

Table 5.6 Sixth set of measurements, L=45.1m, D=10.16cm, d=2.54cm, water temperature 42°C

Point	Inner pipe length (m)	Water level (m)	Water pumping rate (m^3 h^{-1})
1	30.20	39.20	43.5
2	24.20	39.70	38.0
3	18.20	39.80	31.0
4	12.20	40.20	19.0

Table 5.7 Seventh set of measurements, L=24.3m, D=7.62cm, d=1.27cm, water temperature 42°C

Point	Inner pipe length (m)	Water level (m)	Water pumping rate (m^3 h^{-1})
1	24.10	11.30	9.4
2	23.30	11.40	8.4
3	22.80	11.40	8.2
4	21.80	11.50	7.4
5	20.30	11.70	5.5

Table 6.1 Comparison of both models - % mean error

Measurement set	Mean void fraction model	Integral model
1	29.6 (9.3)	11.3 (7.4)
2	51.9 (2.8)	13.5 (6.5)
3	136.2 (4.7)	29.6 (23.6)
4	66.1 (10.2)	16.3 (8.4)
5	49.2 (4.5)	16.2 (13.7)
6	43.1 (3.6)	27.7 (7.7)
7	47.2 (2.5)	6.1 (4.8)

Figure Captions

Figure 3.1: Airlift pumping system

Figure 3.2: External and internal air delivery systems

Figure 4.1: Definition of cells in the upriser pipe

Figure 4.2: Example of a flow regime map, [10].

Figure 6.1: Influence of cell grid on the void fraction profile in the upriser. Simulations pertain to point 6 of Table 5.1.

Figure 6.2: Comparison of models with experiment: First data set

Figure 6.3: Comparison of models with experiment: Second data set

Figure 6.4: Comparison of models with experiment: Third data set

Figure 6.5: Comparison of models with experiment: Fourth data set

Figure 6.6: Comparison of models with experiment: Fifth data set

Figure 6.7: Comparison of models with experiment: Sixth data set

Figure 6.8: Comparison of models with experiment: Seventh data set

Figure 6.9: Mean void fraction model vs. experimental water pumping rate ($m^3\ h^{-1}$)

Figure 6.10: Integral model vs. experimental water pumping rate ($m^3\ h^{-1}$)

Figure 6.11: Mean error (%) of models for each experimental data set

Extended Summary

A model is developed for the simulation of airlift pumps for moderate-depth water wells. The latter are used when other more efficient types cannot be used, such as geothermal mining [1], deep-sea mining [5] and waste treatment [2]. Simplicity, versatility and lack of moving mechanical parts are its main advantages. An airlift pump usually consists of a pipe, part of which is submerged in the well (Fig 3.1). A compressor injects air via an air line either externally or internally. Water flows through the suction section (*1* thru *i*), mixes with air and flows out through the upriser section (*i* thru *2*). Maximum efficiency is achieved when the air-water mixture in the upriser has the slug flow pattern.

A model currently in use, the so-called *mean void fraction model* was proposed by Kato et al, [8]. Unfortunately, this model is inadequate for well depths greater than 11 meters, due to the usage of low accuracy correlations and to the assumption of one flow regime along the upriser. The model proposed here, which is referred to as *integral model*, resolves the above problems. It is based on the division of the upriser into "cells" (Fig.4.1) and application of a momentum balance to each one. This set of momentum balances together with equation 4.14 consist a system of equations which is solved for pressure (along the upriser) and water (or air) mass flow. Friction pressure drop and void fraction are calculated from correlations, which depend on the flow regime existing in each cell. The regime is determined from a map proposed by Taitel et al [10], with a slight modification: regions (instead of lines) are used for the regime transitions. This ensures numerical stability by achieving smooth changes in frictional pressure drop. Otherwise, there are discontinuities ("jumps") with change of correlation.

The mean void fraction and integral models were used to predict the water outflow in 7 series of experiments performed by the Institute of Geological Research (IGME). A grid of 25 cells (which assures a grid independent solution-Figure 6.1) was used for the integral model.

Simulation results are shown in Figures 6.2 to 6.11. The integral model was in good agreement with experiment, with a maximum error of 29%, while the mean void fraction model gave an error as high as 136%. Even better results can be obtained by using more accurate correlations for void fraction and friction calculation. The main source of error in the integral model is thought to be in the void fraction correlation.

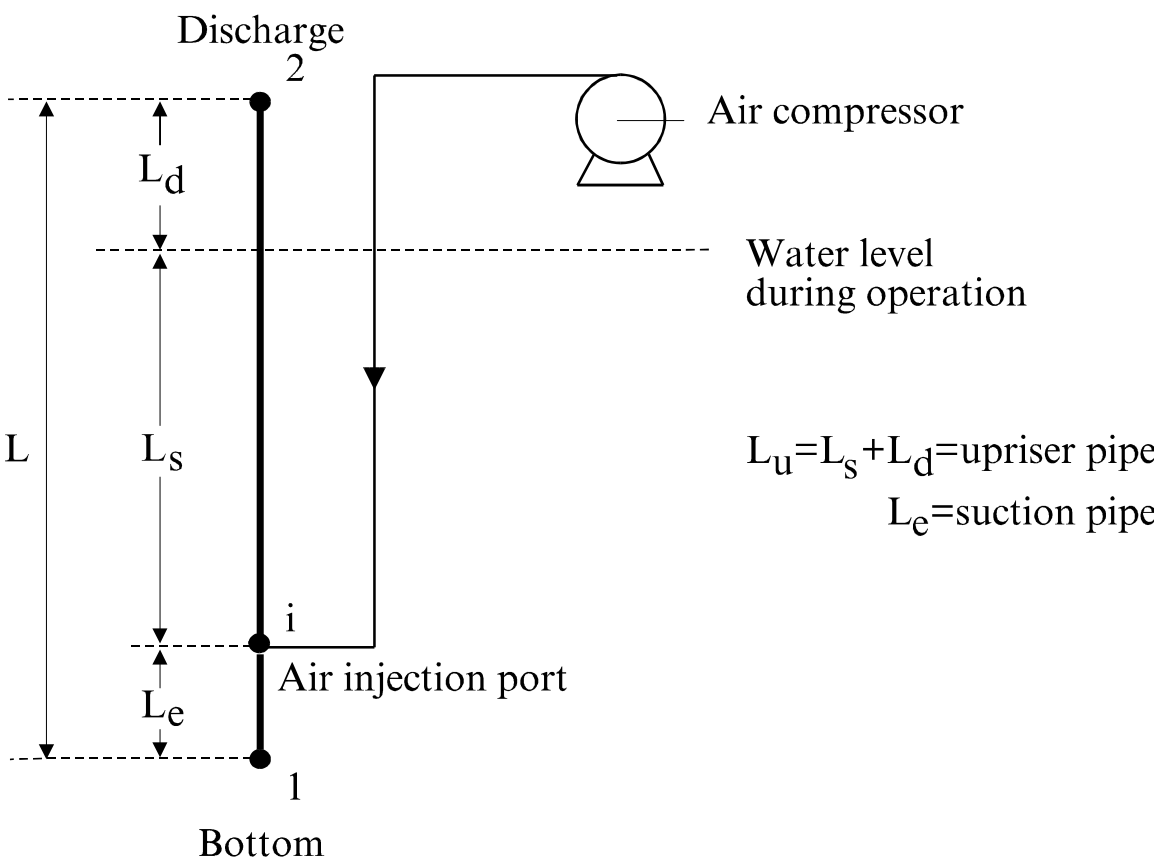
Discharge
2
Air compressor
L_d
Water level
during operation
L
L_s
$L_u=L_s+L_d$=upriser pipe
L_e=suction pipe
i
Air injection port
L_e
1
Bottom

Figure 3.1

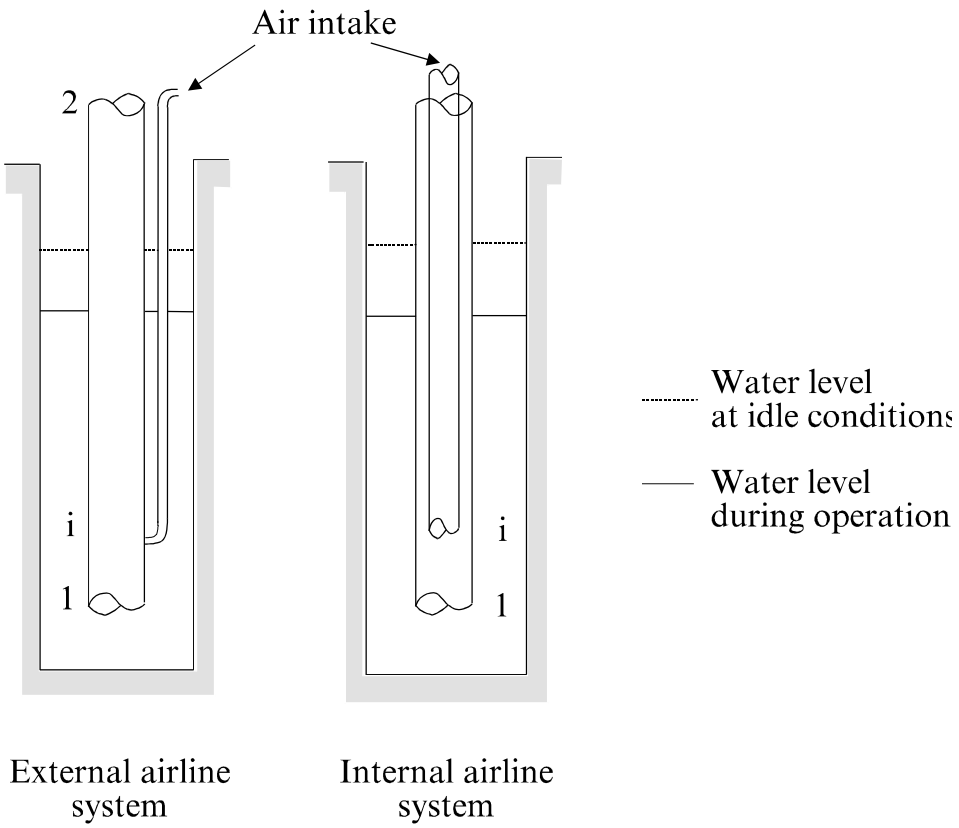
Air intake
2
i
1
i
1
Water level
at idle conditions
Water level
during operation
External airline
system
Internal airline
system

Figure 3.2

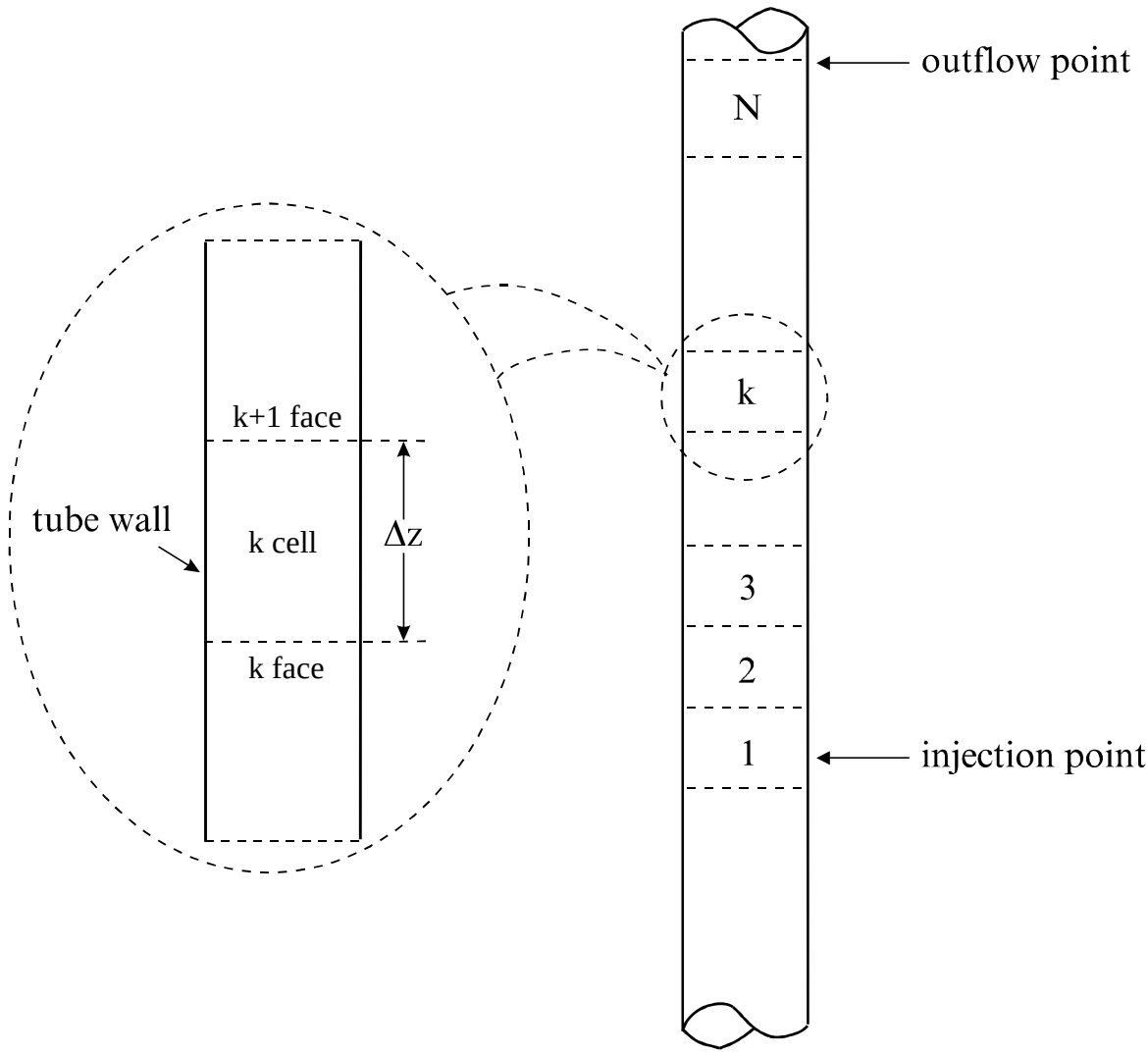
outflow point
N
k
3
2
1
injection point
k+1 face
tube wall
k cell
Δz
k face

Figure 4.1

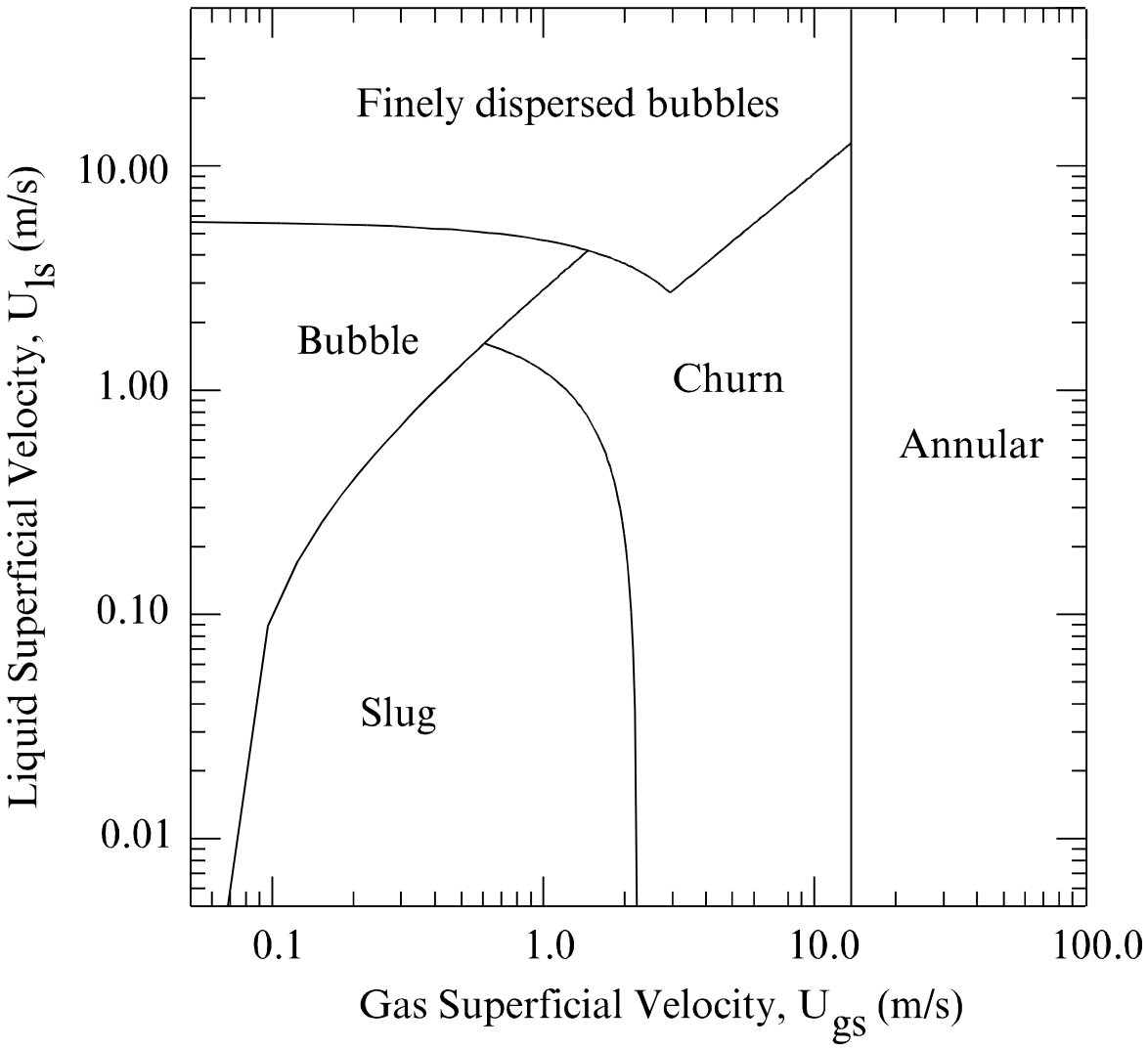
Finely dispersed bubbles
Bubble
Churn
Annular
Slug
10.00
1.00
0.10
0.01
0.1
1.0
10.0
100.0
Liquid Superficial Velocity, U_{ls} (m/s)
Gas Superficial Velocity, U_{gs} (m/s)

Figure 4.2

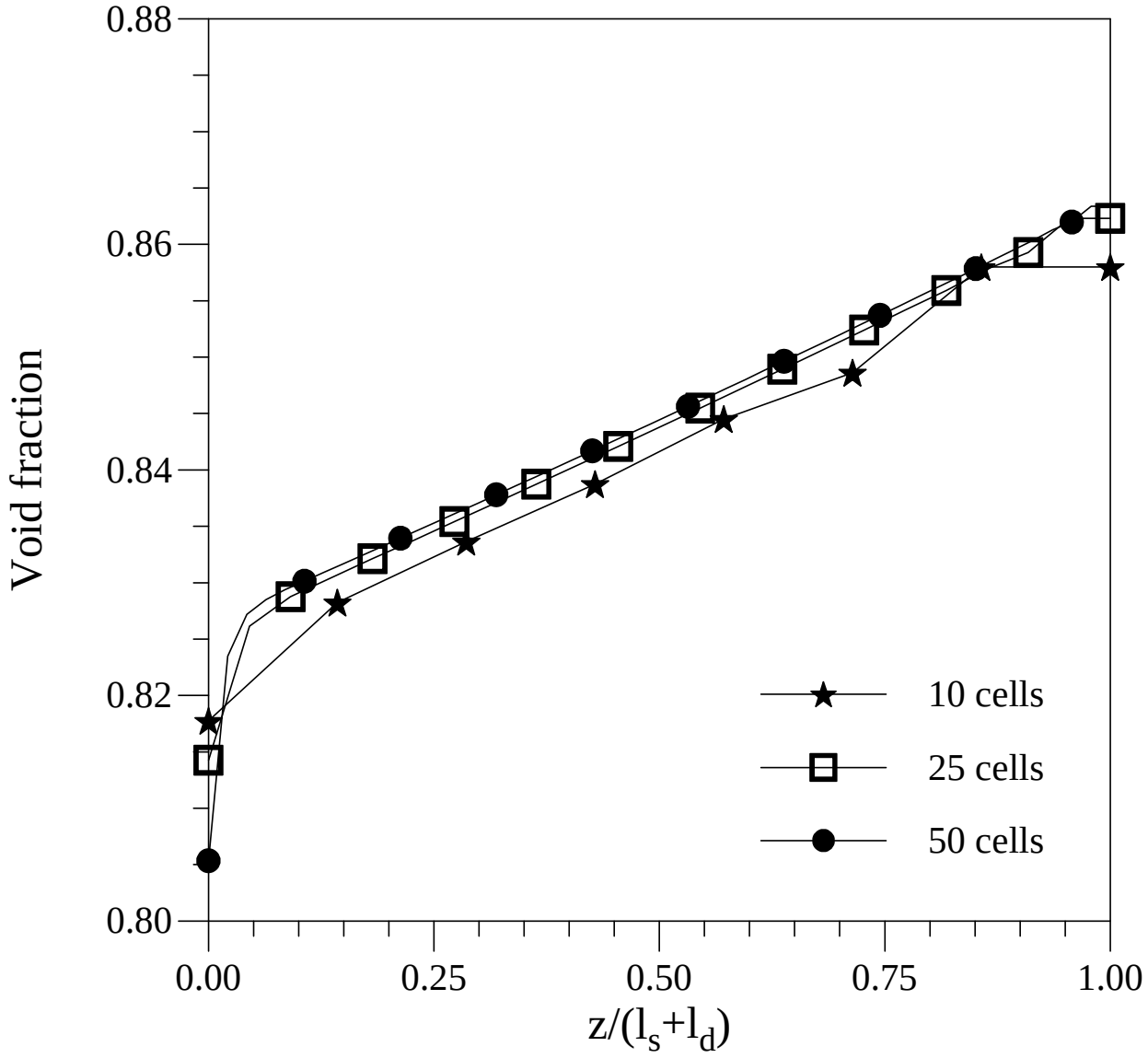
0.88
0.86
0.84
0.82
0.80
Void fraction
0.00
0.25
0.50
0.75
1.00
z/(l_s+l_d)
10 cells
25 cells
50 cells

Figure 6.1

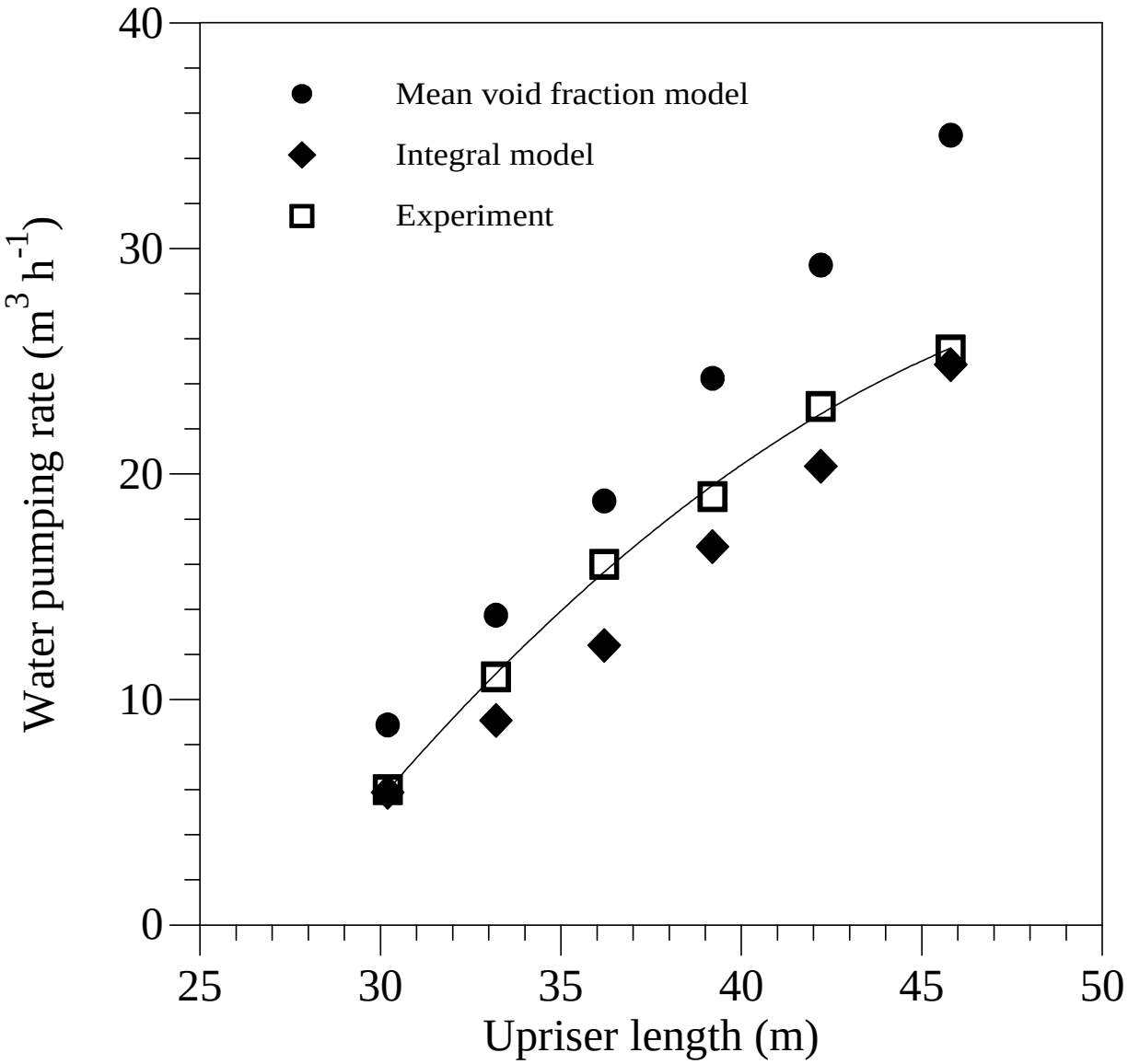
Mean void fraction model
Integral model
Experiment
Water pumping rate (m3 h-1)
Upriser length (m)
0
10
20
30
40
25
30
35
40
45
50

Figure 6.2

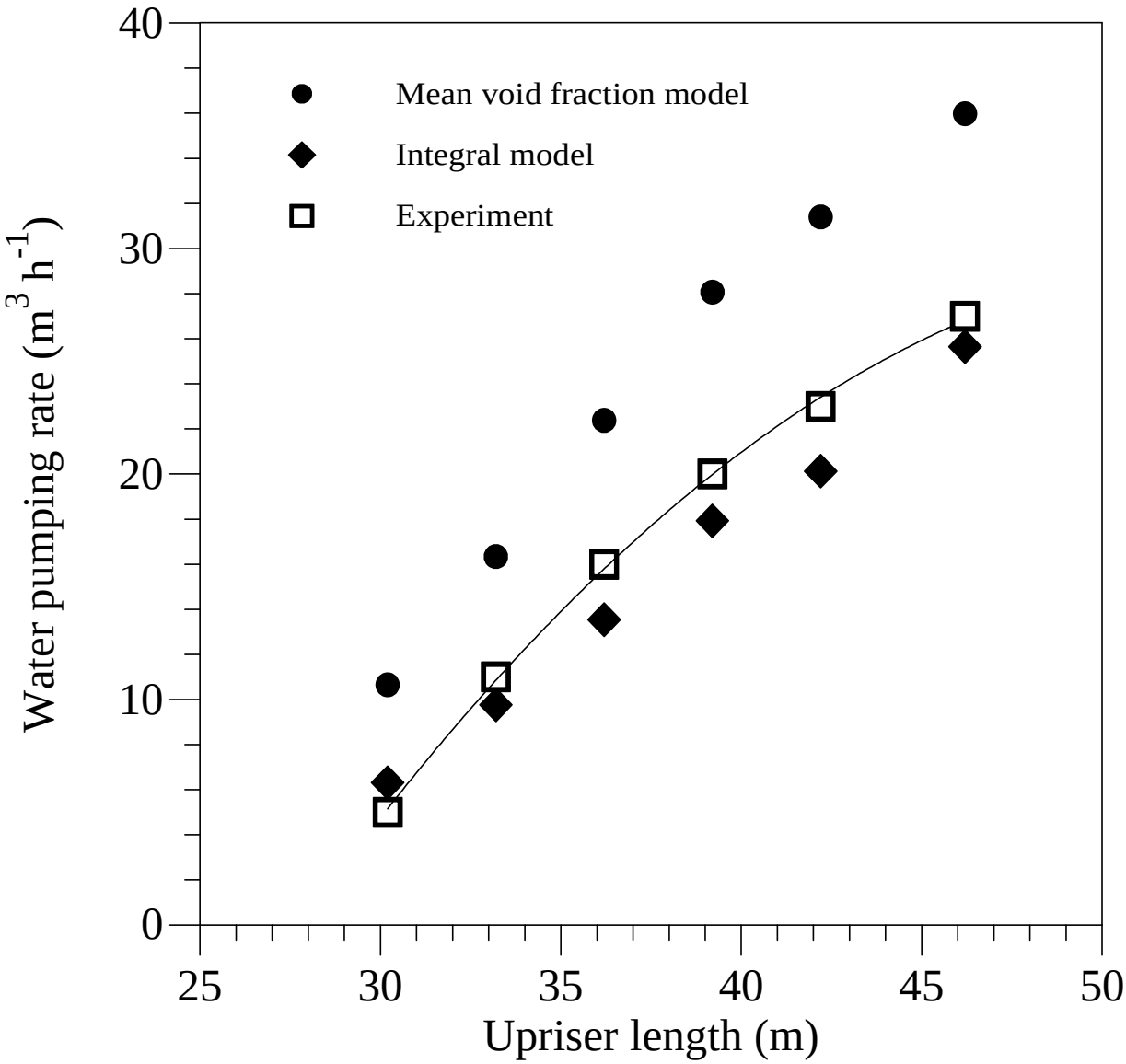
Mean void fraction model
Integral model
Experiment
Water pumping rate (m3 h-1)
Upriser length (m)
0
10
20
30
40
25
30
35
40
45
50

Figure 6.3

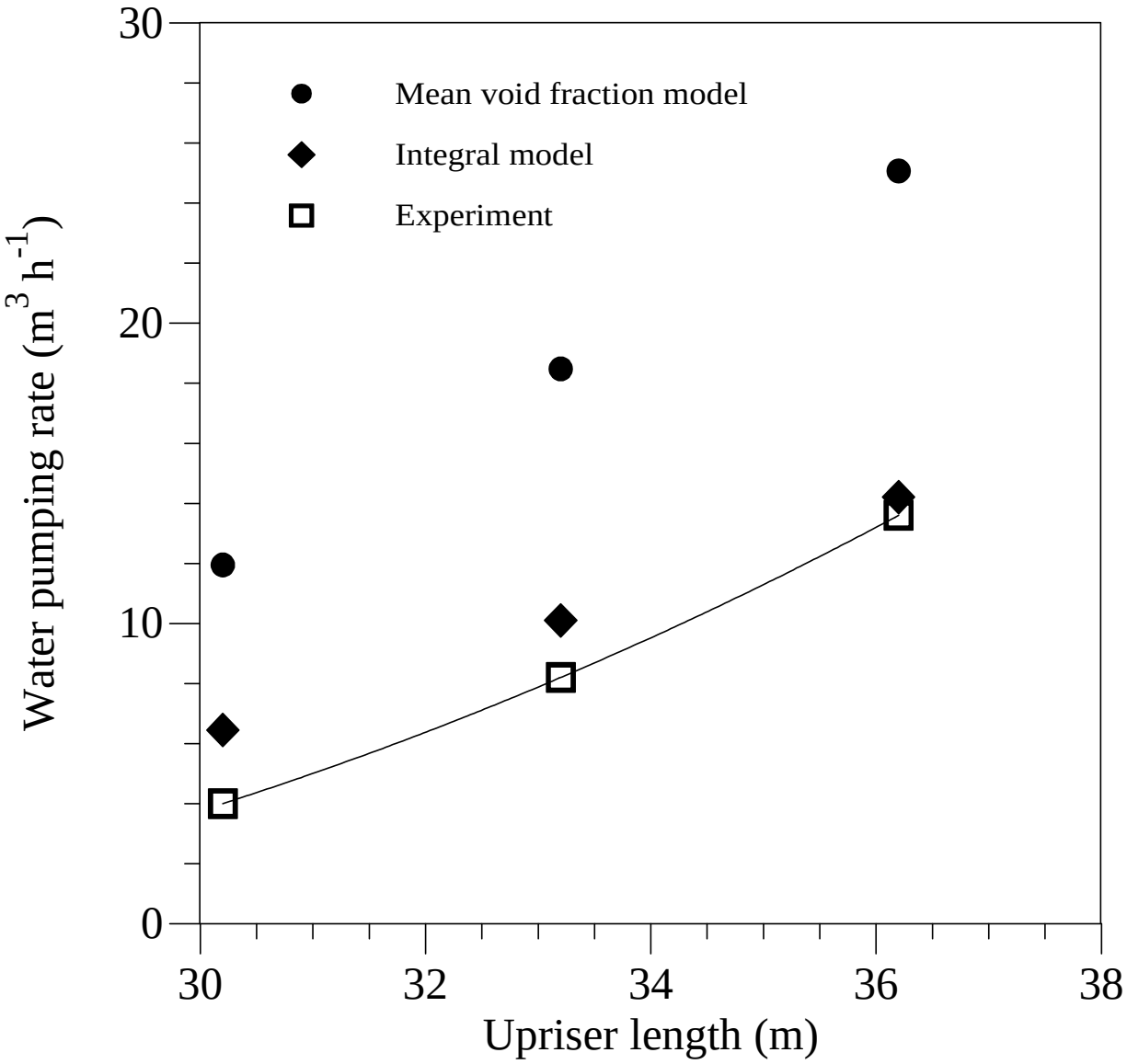
Mean void fraction model
Integral model
Experiment
Water pumping rate (m3 h-1)
Upriser length (m)
0
10
20
30
30
32
34
36
38

Figure 6.4

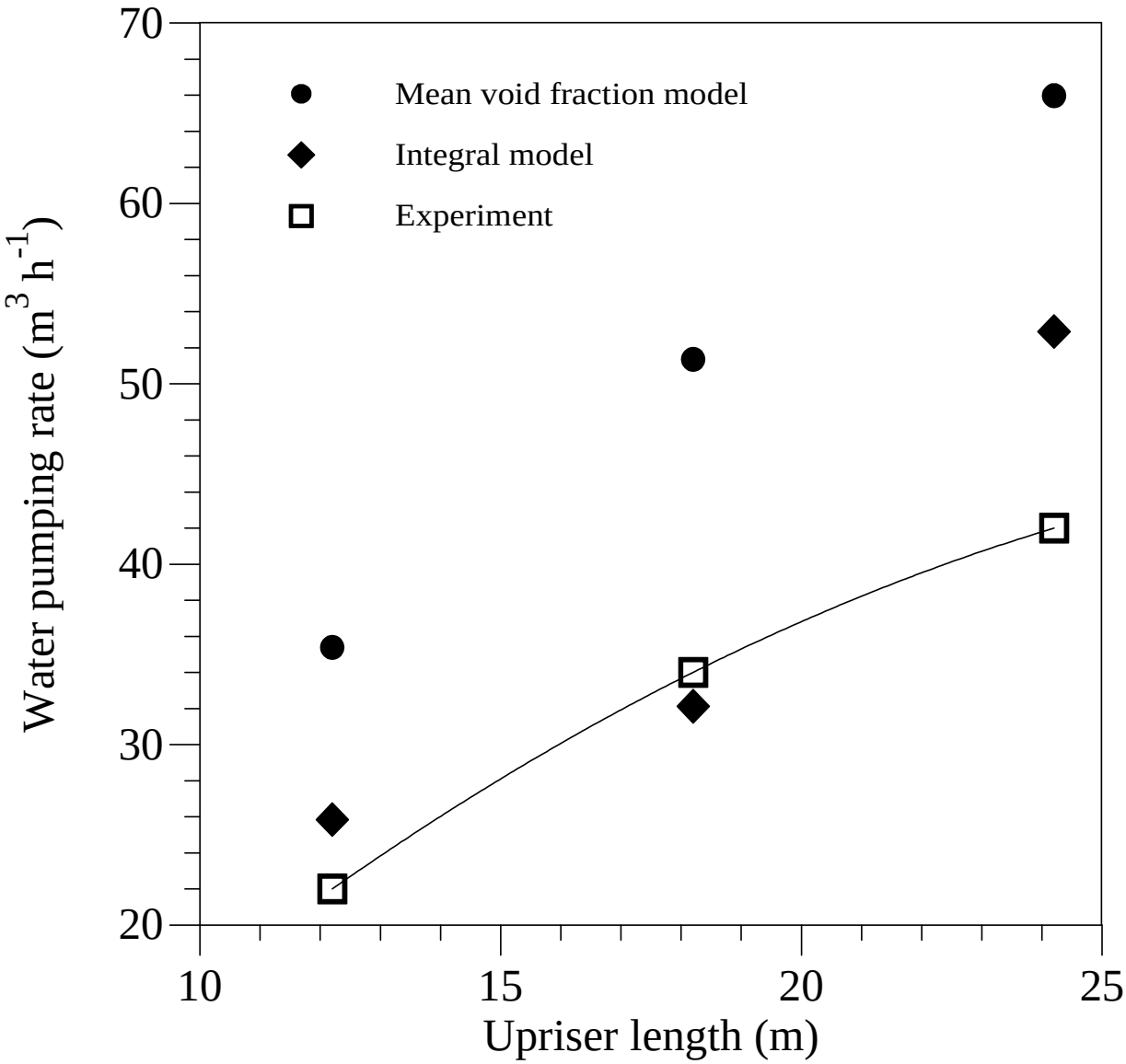
Mean void fraction model
Integral model
Experiment
Water pumping rate (m3 h-1)
Upriser length (m)
70
60
50
40
30
20
10
15
20
25

Figure 6.5

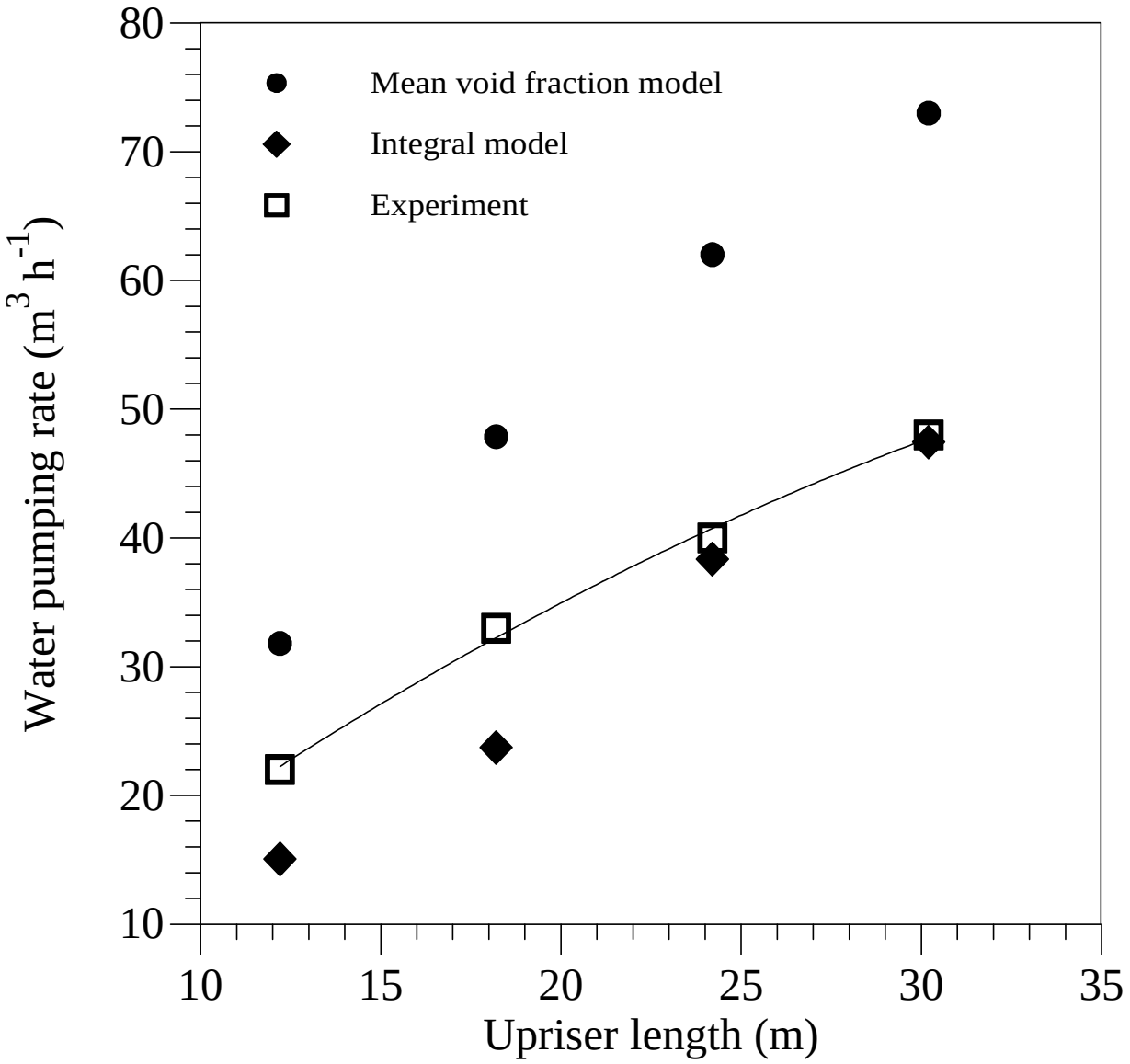
Mean void fraction model
Integral model
Experiment
Water pumping rate (m3 h-1)
Upriser length (m)
80
70
60
50
40
30
20
10
10
15
20
25
30
35

Figure 6.6

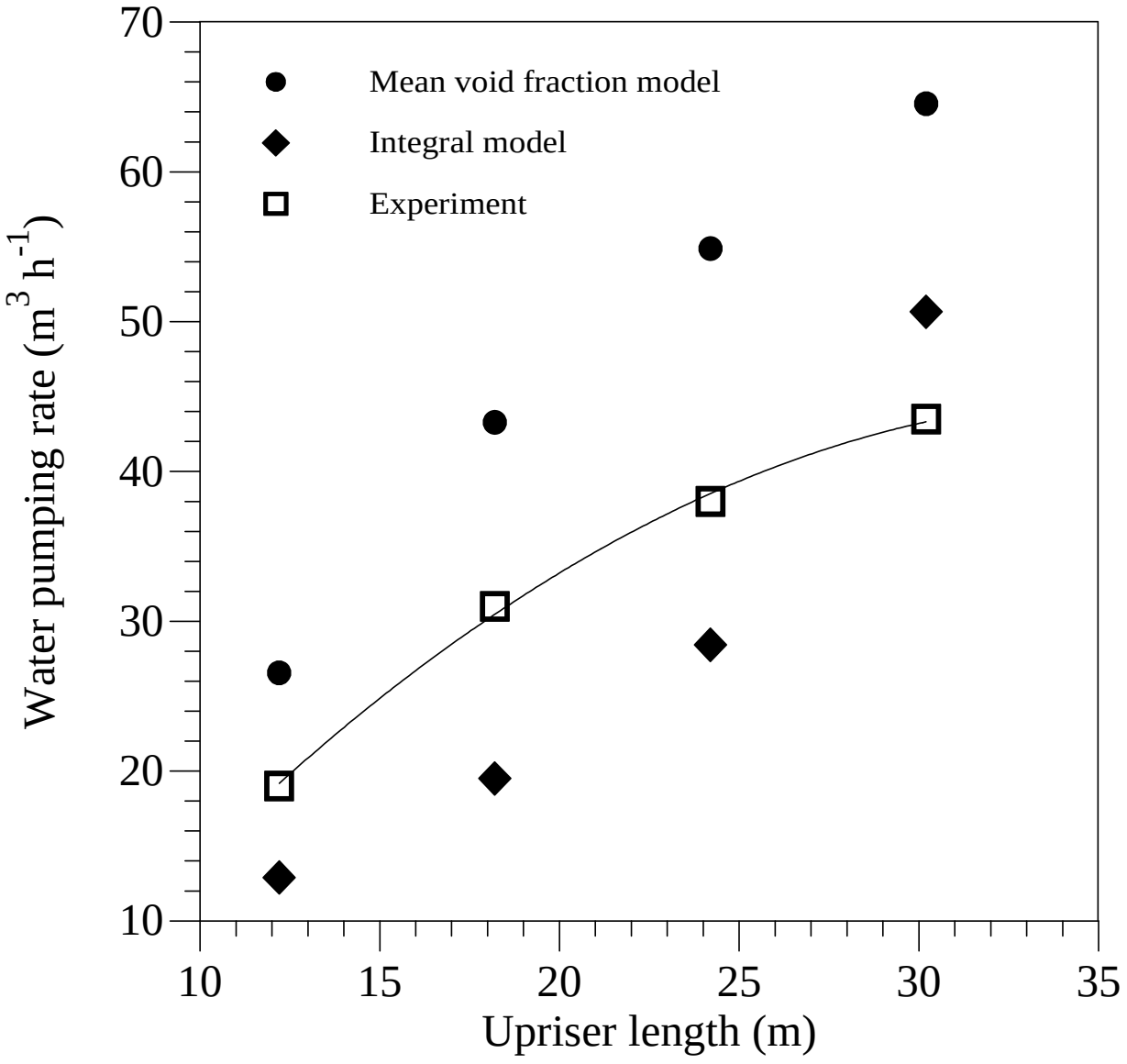
Mean void fraction model
Integral model
Experiment
Water pumping rate (m3 h-1)
Upriser length (m)
70
60
50
40
30
20
10
10
15
20
25
30
35

Figure 6.7

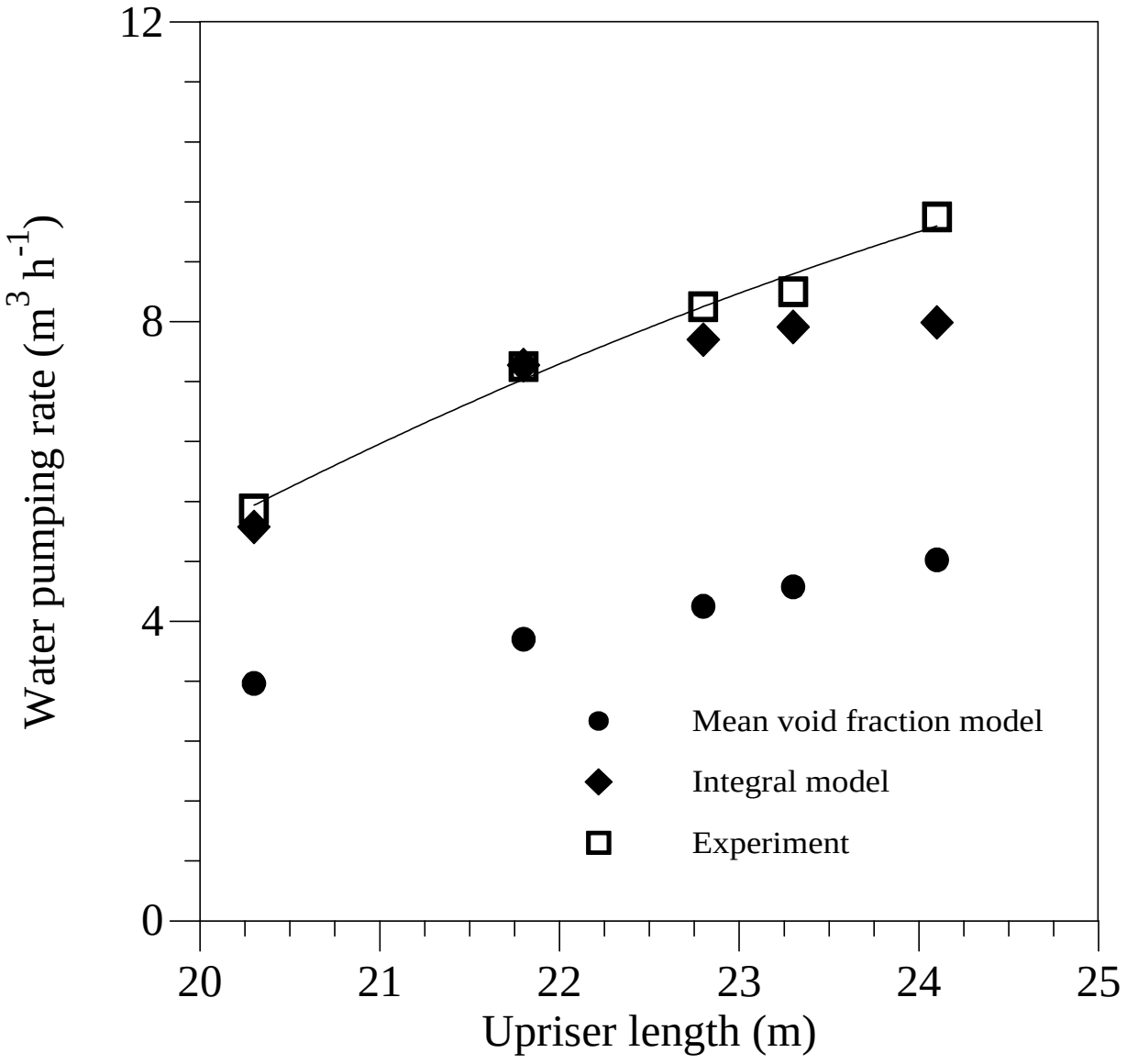
12
8
4
0
20
21
22
23
24
25
Water pumping rate (m3 h-1)
Upriser length (m)
Mean void fraction model
Integral model
Experiment

Figure 6.8

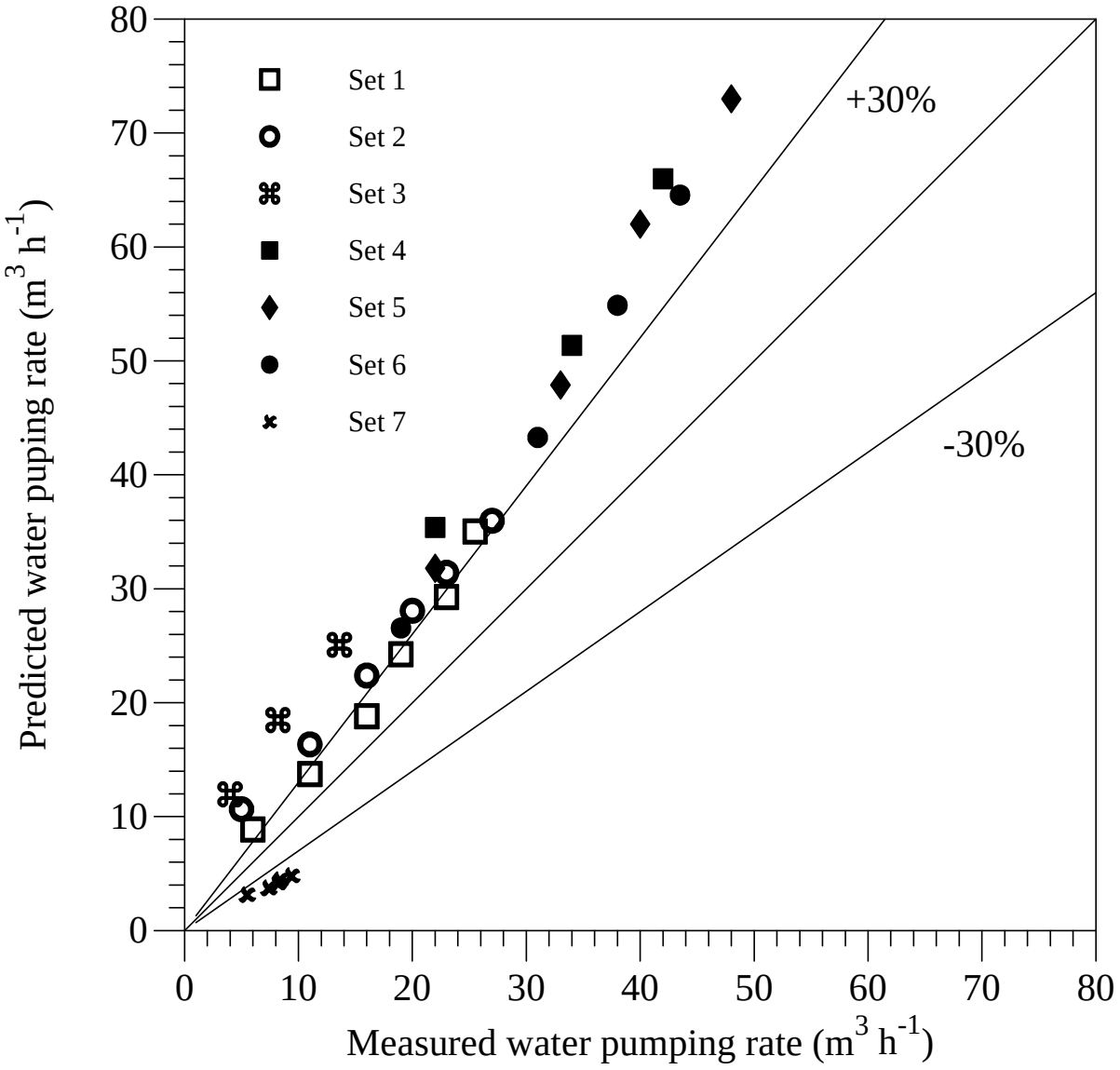
Set 1
Set 2
Set 3
Set 4
Set 5
Set 6
Set 7
+30%
-30%
Predicted water puping rate (m3 h-1)
Measured water pumping rate (m3 h-1)
0
10
20
30
40
50
60
70
80

Figure 6.9

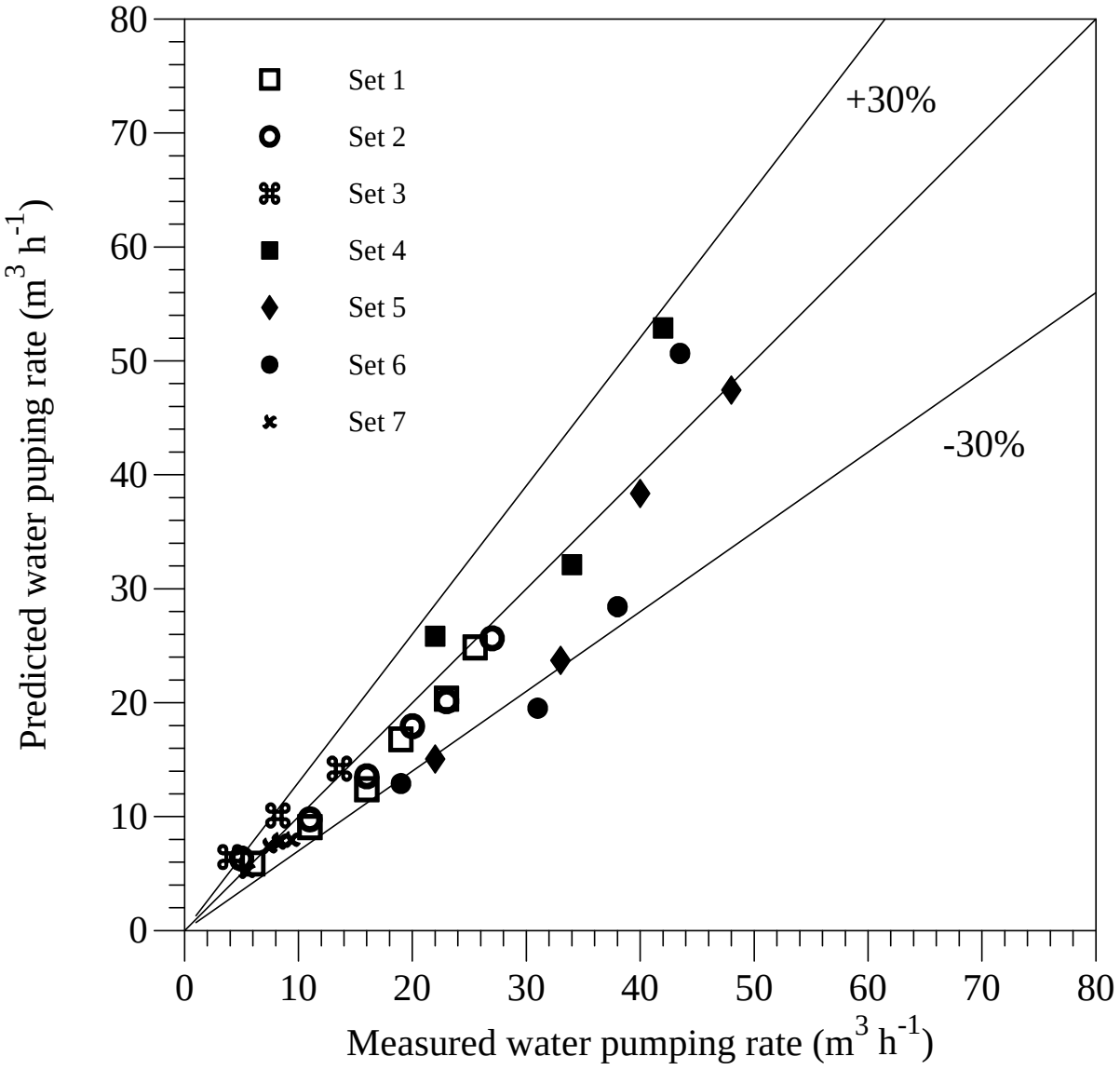
Set 1
Set 2
Set 3
Set 4
Set 5
Set 6
Set 7
+30%
-30%
Predicted water puping rate (m3 h-1)
Measured water pumping rate (m3 h-1)
0
10
20
30
40
50
60
70
80

Figure 6.10

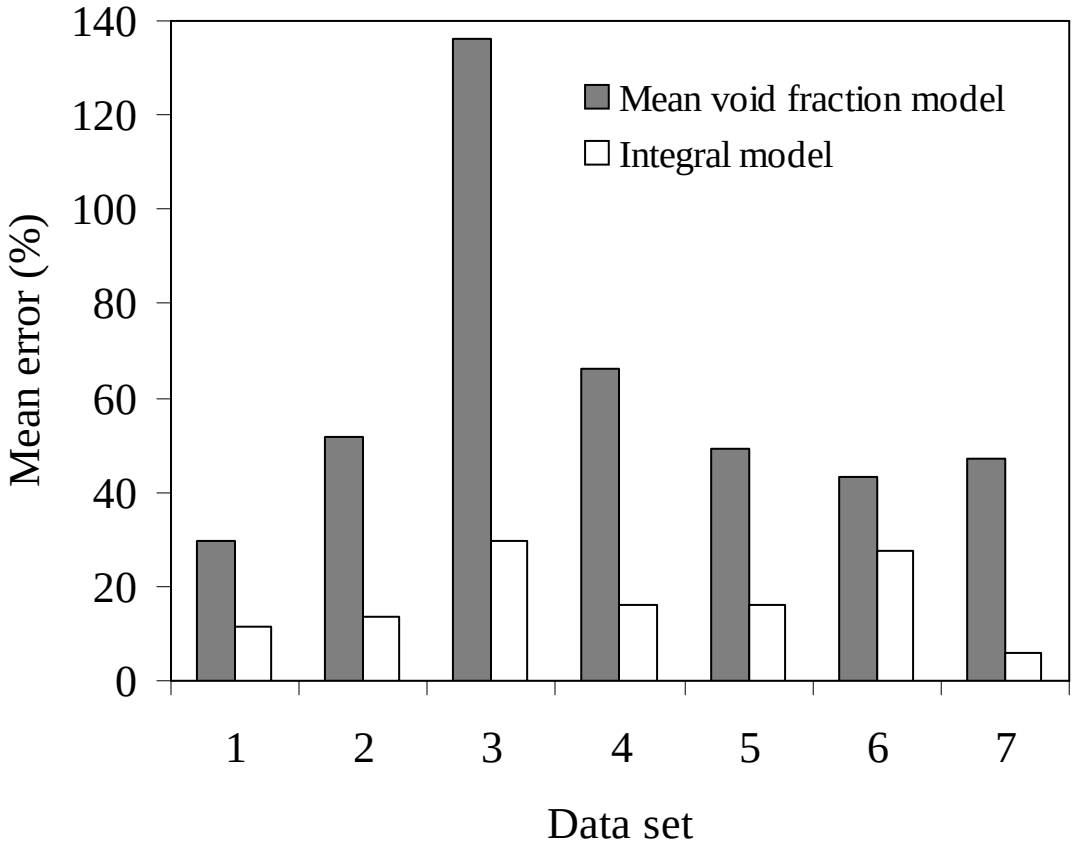
140
120
100
80
60
40
20
0
Mean error (%)
Mean void fraction model
Integral model
1
2
3
4
5
6
7
Data set

Figure 6.11